PROCEEDINGS A

royalsocietypublishing.org/journal/rspa

Research

Cite this article: Bao H, Tan Q, Zhou P, Chen W, Zhang X, Zhong S. 2025 On the Gaussian beam tracing method for long-distance sound wave propagation in non-uniform mean flows. *Proc. R. Soc. A* **481**: 20240485.
https://doi.org/10.1098/rspa.2024.0485

Received: 1 July 2024
Accepted: 13 December 2024

Subject Category:
Engineering

Subject Areas:
mechanical engineering

Keywords:
sound propagation, non-uniform flows, Gaussian beam tracing

Author for correspondence:
Xin Zhang
e-mail: aexzhang@ust.hk

On the Gaussian beam tracing method for long-distance sound wave propagation in non-uniform mean flows

Hongsen Bao[1], Qichen Tan[1], Peng Zhou[1], Wangqiao Chen[1], Xin Zhang[1] and Siyang Zhong[2]

[1]The Hong Kong University of Science and Technology, Clear Water Bay, Kowloon, Hong Kong SAR, People's Republic of China
[2]The Hong Kong Polytechnic University, Hung Hom, Kowloon, Hong Kong SAR, People's Republic of China

HB, 0009-0001-6810-2498

This paper presents an improved Gaussian beam tracing method to efficiently compute long-distance sound wave propagation in non-uniform mean flows. New dynamic ray tracing equations are derived from the convected wave equation in the vicinity of the ray path under the high-frequency asymptotic and paraxial conditions, based on which the solutions of acoustic potential and the corresponding Gaussian beams are developed. The sound pressure at the observer is accurately computed by an integral superposition of all vicinal beams, through a revised weighting function that considers the convection effect on each beam. The proposed method is valid at caustics and can capture the wave diffractions at different sound frequencies. Benchmark problems of the acoustic monopole radiation and the broadband pulse propagation in a free space uniform flow, sound wave interactions with a semi-infinite rigid plate in a moving medium, sound propagations in inhomogeneous stratified flows and in a large-scale vortex flow are studied to validate the proposed method. The results are compared with analytical solutions and high-fidelity numerical results using the finite element method or the fast field program. Good agreements are obtained, showing its potential for the effective assessment of the long-distance sound propagation in complex inhomogeneous flows.

THE ROYAL SOCIETY PUBLISHING

royalsocietypublishing.org/journal/rspa Proc. R. Soc. A 481: 20240485

1. Introduction

Efficient computation of the long-distance sound wave propagation in complex environments is challenging since the inhomogeneities of the medium density, sound speed and flow velocity can cause complex phenomena of sound wave refraction, interference, diffraction and scattering. Usually, these mechanisms can be accounted for by the linearized Euler equations or linearized Navier–Stokes equations, which can be numerically studied by the finite element method (FEM) [1] or finite difference method [2]. However, the computational costs of these methods can be prohibitively expensive for the high-frequency sound wave propagation in large domains to meet the grid resolution requirements for resolving acoustic waves. To this end, the fast field program (FFP) was proposed for the long-distance sound propagation computations [3–5], which, however, is only applicable for the horizontally homogeneous medium and uniform boundary impedance [6], limiting its applicability in general problems. Later, the parabolic equation (PE) method considering the medium inhomogeneity, turbulence and boundary impedance variation was proposed [7]. However, the PE method is inaccurate for high elevation angles due to the effective sound speed approximation [8], and the computational cost can also be high for the high-frequency and long-distance problems since numerical grids are still needed.

An efficient approach to model the sound propagation is based on the ray acoustics theory [9–11], which is naturally suitable for the high-frequency and large-domain problems. The ray acoustics can be derived based on the linearized Euler equations [10], which, under the high-frequency asymptotic condition, are approximated to the eikonal equation and wave action equation to compute the ray path and sound pressure amplitude. The method can efficiently describe the sound wave refraction, interference, transmission and reflection in inhomogeneous acoustic media with complex boundary conditions [8]. Compared with the FFP and PE methods, the ray acoustic method is capable of handling complex environmental states while the computational cost is much lower. However, the standard ray acoustic method cannot capture the sound field at caustics or in shadow zones [8]. To address this issue, Červený *et al*. [12,13] proposed the Gaussian beam tracing (GBT) method in quiescent media, which models the ray path as a finite width beam, and the amplitude of which decreases with the perpendicular distance to the ray in a Gaussian distribution form. At a given observer, the sound pressure field is obtained by integrating the contributions of all vicinal Gaussian beams. The GBT method has advantages of avoiding the singularities at caustics and sharp intensity transitions at the shadow zone boundaries. It also has the capability of computing the sound scattering and diffraction. It is therefore widely used in seismology [13] and marine acoustics [14]. Bian *et al*. [15] implemented this GBT method to model the long-distance noise propagation in inhomogeneous atmospheric environments and set up a complex-valued radiation function to realize the generic directivity pattern of the sound source [16], providing an efficient and accurate approach to evaluate the large domain sound propagation with complex environment conditions.

The existing GBT method is valid only in a quiescent medium. Well-established beam tracing methods to compute the sound fields in non-uniform flows are still lacking. Recently, Yunns *et al*. [17] attempted to model the sound propagation in flows using the dynamic ray tracing (DRT) equations proposed by Červený & Pšenčík [18] for the seismic body wave propagation in anisotropic quiescent media. However, the validity of this approach needs to be reconsidered since the application of the displacement vector equation to the sound pressure leads to the inconsistent solution with the standard ray acoustics. A more physically proper derivation of the DRT equations to account for the flow effect was proposed by Chen *et al*. [19] based on the high-frequency asymptotic wave equation proposed by Ostashev *et al*. [20]. However, the effect of the wavefront curvature variation and the dependence of beam width on the wave frequency are ignored when building the Gaussian beam. As a result, the wave diffraction and scattering phenomena at different sound frequencies are not captured.

royalsocietypublishing.org/journal/rspa Proc. R. Soc. A 481: 20240485

This work aims at developing an improved GBT method in non-uniform mean flows in a more systematic approach. A new wavefront orthogonal coordinate system is established along the ray path accounting for the flow effects. In this coordinate system, new DRT equations are derived based on the convected wave equation. The paraxial solutions of the acoustic potential and paraxial Gaussian beams are developed by solving the DRT equations. The sound pressure at the observer is accurately computed by an integral superposition of all vicinal beams, through a revised weighting function that considers the convection effect on each beam. The paraxial phase difference due to the wavefront curvature and the dependence of the beam width on the sound frequency are considered. All steps are rigorously derived except for the high-frequency assumption that is necessary for the geometric acoustics-based methods.

In the following contents, the detailed methodology and equations are presented in §2. The feasibility, reliability and accuracy of the proposed GBT method for the sound wave propagation in flows are studied in §3, by comparisons with the analytical solutions and the numerical results. The conclusion and summary of this work are given in §4.

2. Methodology

In this section, the detailed GBT method for the sound wave propagations in inhomogeneous flows is presented. The method contains four main steps. First, in §2a the acoustic ray paths are solved by the ray tracing equations, and the new wavefront orthogonal coordinate system associated with each ray is established. Second, in §2b the new DRT equations are derived to solve the acoustic velocity potential along the rays. Third, in §2c the complex-valued solution of the DRT equations is developed to construct the Gaussian beams. Fourth, in §2d the beam summation formula considering the flow effect is proposed to compute the sound pressure at arbitrary observers. In §2e, the correction on sound attenuation due to the medium absorption is discussed. And in §2f, the time-domain GBT method is presented to compute the broadband pulse propagations in moving acoustic media.

(a) Wavefront orthogonal coordinate system

The derivation starts from the eikonal equation in inhomogeneous non-dissipative flows proposed by Pierce [10,11]. For a steady, continuous and inhomogeneous medium, we denote the flow velocity and sound speed distributions as $\boldsymbol{u}(\boldsymbol{x})$ and $c(\boldsymbol{x})$, respectively. For the acoustic velocity potential function Φ, we use the monochromatic one-way wave propagation ansatz [21]

$$\Phi = \phi \exp(\mathrm{i}\omega T), \tag{2.1}$$

where the positive value ω is the acoustic angular frequency, $\mathrm{i} = \sqrt{-1}$ is the imaginary unit and T is the travel time, i.e. the eikonal. By substituting this expression into the equations (34) to (36) used in [10], we obtain the eikonal equation

$$(\boldsymbol{\nabla} T)^2 = \frac{(1 - \boldsymbol{u} \cdot \boldsymbol{\nabla} T)^2}{c^2}. \tag{2.2}$$

The solution of the eikonal equation is given in terms of ray tracing (RT) equations [11]

$$\frac{\mathrm{d}\boldsymbol{r}}{\mathrm{d}T} = \frac{c^2 \boldsymbol{s}}{1 - \boldsymbol{u} \cdot \boldsymbol{s}} + \boldsymbol{u}, \quad \frac{\mathrm{d}\boldsymbol{s}}{\mathrm{d}T} = -\frac{1 - \boldsymbol{u} \cdot \boldsymbol{s}}{c} \boldsymbol{\nabla} c - \boldsymbol{s} \times (\boldsymbol{\nabla} \times \boldsymbol{u}) - (\boldsymbol{s} \cdot \boldsymbol{\nabla}) \boldsymbol{u}, \tag{2.3}$$

where $\boldsymbol{s} = \boldsymbol{\nabla} T$ is called the wave slowness vector, and $\boldsymbol{r}$ is the ray path. The operator $\mathrm{d}/\mathrm{d}T$ denotes the derivative along the ray path. Based on the slowness vector $\boldsymbol{s}$, we can define the wavefront normal vector

$$\boldsymbol{e}_T = \boldsymbol{s} / |\boldsymbol{s}|^2. \tag{2.4}$$

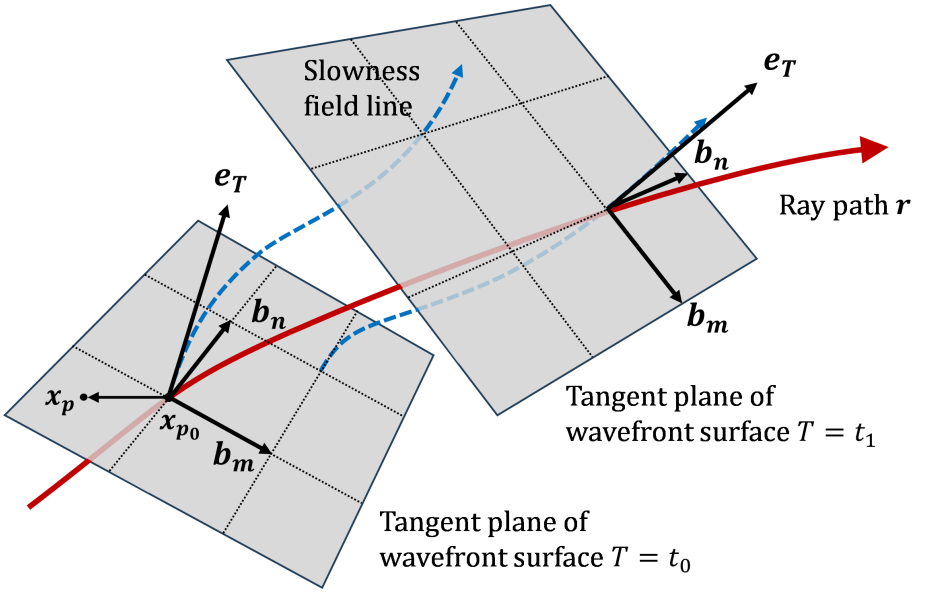

Figure 1. Definition of the wavefront orthogonal coordinate system.

Then, the group velocity vector $\boldsymbol{c_g}$, group velocity c_g and phase velocity c_p can be expressed as

$$\boldsymbol{c_g} = \frac{\mathrm{d}\boldsymbol{r}}{\mathrm{d}T} = c\,|\boldsymbol{s}|\,\boldsymbol{e_T} + \boldsymbol{u}, \quad c_g = |\boldsymbol{c_g}|, \quad c_p = c + |\boldsymbol{s}|\,\boldsymbol{u}\cdot\boldsymbol{e_T}. \tag{2.5}$$

In practice, for the given initial slowness vector $\boldsymbol{s} = \boldsymbol{s_0}$ at the ray path location $\boldsymbol{r} = \boldsymbol{r_0}$, the values of $\boldsymbol{s}$, $\boldsymbol{r}$ with T can be easily obtained by solving the RT equation (2.3).

When the ray path is solved, the wavefront orthogonal coordinate system can be established along the ray. We set one of the basis vectors to be the local wavefront normal vector $\boldsymbol{e_T}$, and the corresponding coordinate is T.

On the tangent plane of the wavefront surface, we choose orthonormal unit vectors $\boldsymbol{b_m}$, $\boldsymbol{b_n}$ as the other two basis vectors. A schematic of the new coordinate system is shown in figure 1. The unit vectors satisfy the following differential equations

$$\frac{\partial \boldsymbol{b_m}}{\partial T} = a_m \boldsymbol{s}, \quad \frac{\partial \boldsymbol{b_n}}{\partial T} = a_n \boldsymbol{s}, \tag{2.6}$$

where a_m, a_n are continuous functions of T. If ($\boldsymbol{e_T}$, $\boldsymbol{b_m}$, $\boldsymbol{b_n}$) is a mutually perpendicular right-handed triplet of vectors at an initial point $T = T_0$, it will form a mutually perpendicular right-handed triplet of vectors at any point along the slowness field line. The coefficients a_m, a_n in equation (2.6) can be determined through the equations (2.7) to (2.12).

Due to the orthogonality, it is easy to know $\boldsymbol{b_m}\cdot\boldsymbol{s} = 0$, so that

$$\frac{\partial}{\partial T}(\boldsymbol{b_m}\cdot\boldsymbol{s}) = \frac{\partial \boldsymbol{b_m}}{\partial T}\cdot\boldsymbol{s} + \boldsymbol{b_m}\cdot\frac{\partial \boldsymbol{s}}{\partial T} = 0. \tag{2.7}$$

Multiplying equation (2.6) by $\boldsymbol{s}$, and using the relationship $|\boldsymbol{s}| = 1/c_p$, we obtain

$$\frac{\partial \boldsymbol{b_m}}{\partial T}\cdot\boldsymbol{s} = a_m \boldsymbol{s}\cdot\boldsymbol{s} = \frac{a_m}{c_p^2}. \tag{2.8}$$

Substituting equation (2.8) into (2.7), yields

$$a_m = -c_p^2\left(\boldsymbol{b_m}\cdot\frac{\partial \boldsymbol{s}}{\partial T}\right). \tag{2.9}$$

Similarly, for a_n, we obtain

$$a_n = -c_p^2\left(\boldsymbol{b_n}\cdot\frac{\partial \boldsymbol{s}}{\partial T}\right). \tag{2.10}$$

Meanwhile, with the identity $(\boldsymbol{s}\cdot\nabla)\boldsymbol{s} = -\boldsymbol{s}\times(\nabla\times\boldsymbol{s}) + \frac{1}{2}\nabla|\boldsymbol{s}|^2$, and $\nabla\times\boldsymbol{s} = \boldsymbol{0}$ because of $\boldsymbol{s} = \nabla T$, we have

$$\frac{\partial \boldsymbol{s}}{\partial T} = (\boldsymbol{e_T}\cdot\nabla)\boldsymbol{s} = c_p^2(\boldsymbol{s}\cdot\nabla)\boldsymbol{s} = \frac{1}{2}c_p^2\nabla|\boldsymbol{s}|^2 = \frac{1}{2}c_p^2\nabla\left(\frac{1}{c_p^2}\right) = -\frac{1}{c_p}\nabla c_p. \tag{2.11}$$

Finally, taking equation (2.11) into (2.9) and (2.10), we obtain

$$\frac{\partial \boldsymbol{b_m}}{\partial T} = \frac{1}{c_p}\frac{\partial c_p}{\partial m}\boldsymbol{e_T}, \quad \frac{\partial \boldsymbol{b_n}}{\partial T} = \frac{1}{c_p}\frac{\partial c_p}{\partial n}\boldsymbol{e_T}. \tag{2.12}$$

Thus, the wavefront orthogonal coordinate system with basis vectors $(\boldsymbol{e_T}, \boldsymbol{b_m}, \boldsymbol{b_n})$ is completely defined, and the corresponding coordinates are (T, m, n).

The position vector of a point $\boldsymbol{x_p}$ can be expressed as

$$\boldsymbol{x_p} = \boldsymbol{x_{p_0}} + \boldsymbol{b_m}m + \boldsymbol{b_n}n, \tag{2.13}$$

where $\boldsymbol{x_{p_0}}$ is an adjacent point located on the ray path and on the same wavefront surface with $\boldsymbol{x_p}$, as shown in figure 1. Performing the total derivative to the equation (2.13) leads to

$$\begin{aligned}\mathrm{d}\boldsymbol{x_p} &= \frac{\partial \boldsymbol{x_{p_0}}}{\partial T}\mathrm{d}T + m\frac{\partial \boldsymbol{b_m}}{\partial T}\mathrm{d}T + n\frac{\partial \boldsymbol{b_n}}{\partial T}\mathrm{d}T + \boldsymbol{b_m}\mathrm{d}m + \boldsymbol{b_n}\mathrm{d}n \\ &= \left(1 + m\frac{1}{c_p}\frac{\partial c_p}{\partial m} + n\frac{1}{c_p}\frac{\partial c_p}{\partial n}\right)\boldsymbol{e_T}\mathrm{d}T + \boldsymbol{b_m}\mathrm{d}m + \boldsymbol{b_n}\mathrm{d}n.\end{aligned} \tag{2.14}$$

Therefore, the Lamé coefficients of the proposed coordinate system are $(h, 1, 1)$ with

$$h = \left|\left(1 + m\frac{1}{c_p}\frac{\partial c_p}{\partial m} + n\frac{1}{c_p}\frac{\partial c_p}{\partial n}\right)\boldsymbol{e_T}\right| = \left(c_p + m\frac{\partial c_p}{\partial m} + n\frac{\partial c_p}{\partial n}\right). \tag{2.15}$$

For the differential equations of the base vectors $\boldsymbol{b_m}, \boldsymbol{b_n}$ along the ray path, similar derivation can be performed referring to the process from the equations (2.7) to (2.10). The results are

$$\frac{\mathrm{d}\boldsymbol{b_m}}{\mathrm{d}T} = -\left(\boldsymbol{b_m}\cdot\frac{\mathrm{d}\boldsymbol{s}}{\mathrm{d}T}\right)\boldsymbol{e_T}, \quad \frac{\mathrm{d}\boldsymbol{b_n}}{\mathrm{d}T} = -\left(\boldsymbol{b_n}\cdot\frac{\mathrm{d}\boldsymbol{s}}{\mathrm{d}T}\right)\boldsymbol{e_T}, \tag{2.16}$$

where the value $\mathrm{d}\boldsymbol{s}/\mathrm{d}T$ is obtained from the RT equation (2.3). Equation (2.16) can be solved by specifying any right-handed mutually orthogonal vectors triplet $(\boldsymbol{e_{T_0}}, \boldsymbol{b_{m_0}}, \boldsymbol{b_{n_0}})$ as the initial condition. Therefore, we complete the wavefront orthogonal coordinate system construction along the ray path, with basis vectors $(\boldsymbol{e_T}, \boldsymbol{b_m}, \boldsymbol{b_n})$ obtained from equations (2.4) and (2.16).

(b) Dynamic ray tracing equations in moving media

Having obtained the local wavefront coordinate system, we are now ready to compute the acoustic potential in the vicinity of the ray path. The derivation is based on the monochromatic convected wave equation of the acoustic velocity potential Φ in inhomogeneous non-dissipative flows proposed by Ostashev *et al*. [20]

$$\left[\nabla^2 + \frac{\omega^2}{c^2} + 2\mathrm{i}\frac{\omega}{c^2}\boldsymbol{u}\cdot\nabla - \frac{(\boldsymbol{u}\cdot\nabla)(\boldsymbol{u}\cdot\nabla)}{c^2}\right]\Phi = 0. \tag{2.17}$$

The corresponding sound pressure P is

$$P = \sqrt{\frac{\rho}{\rho_r}}\left(1 + \frac{\mathrm{i}}{\omega}\boldsymbol{u}\cdot\nabla\right)\Phi, \tag{2.18}$$

where ρ is the medium density, and ρ_r is the reference density. To solve equation (2.17), we expressed Φ in the one-way wave propagation form

$$\Phi = \phi(T, m, n)\exp(\mathrm{i}\omega T). \tag{2.19}$$

In the wavefront orthogonal coordinate system along the ray path, we assume m, n as small quantities of the order of $\epsilon \sim O(\omega^{-1/2})$ [13]. To make the derivation tractable, in the vicinity of the ray, it is assumed that the partial derivatives of ϕ in the directions of the base vectors $\boldsymbol{b_m}$, $\boldsymbol{b_n}$, which are on the tangent plane of the wavefront, are approximately equal to zero, i.e.

$$\frac{\partial\phi}{\partial m} \approx 0, \quad \frac{\partial\phi}{\partial n} \approx 0.$$

Along the direction $\boldsymbol{e_T}$, the paraxial approximation $\partial^2\phi/\partial T^2 \approx 0$ is applied, referring to the similar assumption made by Ostashev *et al*. [8] to derive the parabolic equations for acoustic waves. Then, we obtain the paraxial convected wave equation in frequency domain for ϕ

$$E_2\omega^2 + E_1\omega + E_0 = 0, \tag{2.20}$$

$$E_2 = \left(\frac{1}{c^2} - \frac{1}{h^2} - \frac{2u_T}{hc^2} + \frac{u_T^2}{h^2c^2}\right)\phi, \tag{2.21}$$

$$E_1 = \mathrm{i}\phi\left[\frac{1}{h}\frac{\partial}{\partial T}\left(\frac{1}{h}\right) - \frac{u_T}{c^2h}\frac{\partial}{\partial T}\left(\frac{u_T}{h}\right) - \frac{u_m}{c^2}\frac{\partial}{\partial m}\left(\frac{u_T}{h}\right) - \frac{u_n}{c^2}\frac{\partial}{\partial n}\left(\frac{u_T}{h}\right)\right] + 2\mathrm{i}\left[\frac{1}{h^2} + \frac{u_T}{c^2h} - \frac{u_T^2}{c^2h^2}\right]\frac{\partial\phi}{\partial T}, \tag{2.22}$$

$$E_0 = \left[\frac{\partial^2\phi}{\partial m^2} + \frac{\partial^2\phi}{\partial n^2} - \frac{u_m^2}{c^2}\frac{\partial^2\phi}{\partial m^2} - 2\frac{u_mu_n}{c^2}\frac{\partial^2\phi}{\partial m\partial n} - \frac{u_n^2}{c^2}\frac{\partial^2\phi}{\partial n^2}\right] + O(\omega^0), \tag{2.23}$$

where the flow velocity components in $\boldsymbol{b_I}$ direction are expressed as $u_I = \boldsymbol{u}\cdot\boldsymbol{b_I}$, with $I = m, n$. In the $\boldsymbol{e_T}$ direction, we have $u_T = \boldsymbol{u}\cdot\boldsymbol{e_T}/c_p$. The Lamé coefficient h is obtained from equation (2.15).

As m and n are small, referring to the similar procedures applied in [13,19], the phase velocity c_p, flow velocity $\boldsymbol{u}$ and sound speed c can be expressed using the Taylor's series as

$$c_p(T, m, n) = C_p + \frac{\partial C_p}{\partial m}m + \frac{\partial C_p}{\partial n}n + \frac{1}{2}\frac{\partial^2 C_p}{\partial m^2}m^2 + \frac{1}{2}\frac{\partial^2 C_p}{\partial n^2}n^2 + \frac{\partial^2 C_p}{\partial m\partial n}mn + O(\epsilon^3), \tag{2.24}$$

$$\boldsymbol{u}(T, m, n) = \boldsymbol{U} + \frac{\partial\boldsymbol{U}}{\partial m}m + \frac{\partial\boldsymbol{U}}{\partial n}n + O(\epsilon^2), \tag{2.25}$$

$$c(T, m, n) = C + \frac{\partial C}{\partial m}m + \frac{\partial C}{\partial n}n + O(\epsilon^2). \tag{2.26}$$

Now we introduce the new coordinates $\mathbf{g} = [\mu, \eta]$ to replace m and n with

$$\mu = \sqrt{\frac{\omega}{1 - M_m^2}}m, \quad \eta = \sqrt{\frac{\omega}{1 - M_n^2}}n. \tag{2.27}$$

Substituting equations (2.24) to (2.27) into equations (2.20) to (2.23) and keeping the leading order terms of ω, we can get the high-frequency asymptotic paraxial wave equation in the frequency domain

$$\frac{-\mathbf{g}\mathbf{C}\mathbf{g}^{\mathbf{T}}}{CC_p^2}\phi + \frac{2\mathrm{i}}{C_p^2}\frac{\partial\phi}{\partial T} - \mathrm{i}\frac{1}{C_p^3}\phi\frac{\partial C_p}{\partial T} + \frac{2\mathrm{i}U_T}{C^2C_p}\frac{\partial\phi}{\partial T} - \frac{2\mathrm{i}U_T^2}{C_p^2C^2}\frac{\partial\phi}{\partial T} + \frac{\mathrm{i}U_T^2}{C^2C_p^3}\phi\frac{\partial C_p}{\partial T} + \frac{\mathrm{i}U_mU_T}{C_p^2C^2}\phi\frac{\partial C_p}{\partial m} + \frac{\mathrm{i}U_nU_T}{C_p^2C^2}\phi\frac{\partial C_p}{\partial n} + \frac{\partial^2\phi}{\partial\mu^2} + \frac{\partial^2\phi}{\partial\eta^2} - \frac{2M_mM_n}{\sqrt{1 - M_m^2}\sqrt{1 - M_n^2}}\frac{\partial^2\phi}{\partial\mu\partial\eta} = 0, \tag{2.28}$$

royalsocietypublishing.org/journal/rspa Proc. R. Soc. A 481: 20240485

where the background flow Mach number components in the $\boldsymbol{b_I}$ direction are expressed as $M_I = U_I/C$, with $I = m, n$, and the 2×2 matrix $\mathbf{C}$ is expressed as

$$\mathbf{C} = \begin{bmatrix} \left(1 - M_m^2\right)\dfrac{\partial^2 C_p}{\partial m^2} & \sqrt{\left(1 - M_m^2\right)\left(1 - M_n^2\right)}\dfrac{\partial^2 C_p}{\partial m \partial n} \\ \sqrt{\left(1 - M_m^2\right)\left(1 - M_n^2\right)}\dfrac{\partial^2 C_p}{\partial m \partial n} & \left(1 - M_n^2\right)\dfrac{\partial^2 C_p}{\partial n^2} \end{bmatrix}. \tag{2.29}$$

Further, we re-expressed ϕ using the paraxial Gaussian beam ansatz

$$\phi(T, \mu, \eta) = A(T)\exp\left(\frac{\mathrm{i}\omega \mathbf{G}(T)\mathbf{g}^{\mathrm{T}}}{2}\right)\sqrt{C_p(T)}\,. \tag{2.30}$$

Substitute it into equation (2.28), we get the ordinary differential equations for $\mathbf{G}(T)$ and $A(T)$ as

$$\mathbf{C} + C_p\frac{\mathrm{d}\mathbf{G}}{\mathrm{d}T} + CC_p^2\mathbf{G}\mathbf{T}\mathbf{G} = \mathbf{0}, \tag{2.31}$$

$$2CC_p\frac{\mathrm{d}A}{\mathrm{d}T} + \left(\sigma + C^2C_p^2(\mathrm{tr}(\mathbf{T}\mathbf{G}))\right)A = 0. \tag{2.32}$$

The equation (2.31) is the Ricatti's matrix equation. Following the similar derivation by Červený *et al*. [13], it provides the DRT equations for the matrix $\mathbf{G}$

$$\mathbf{G} = \mathbf{P}\mathbf{Q}^{-1}, \tag{2.33}$$

$$\frac{\mathrm{d}\mathbf{Q}}{\mathrm{d}T} = CC_p\mathbf{T}\mathbf{P}, \quad \frac{\mathrm{d}\mathbf{P}}{\mathrm{d}T} = -\frac{\mathbf{C}\mathbf{Q}}{C_p}, \tag{2.34}$$

where the derivative is along the ray path, and the 2×2 matrix $\mathbf{T}$ is

$$\mathbf{T} = \begin{bmatrix} 1 & -\dfrac{M_m M_n}{\sqrt{\left(1 - M_m^2\right)\left(1 - M_n^2\right)}} \\ -\dfrac{M_m M_n}{\sqrt{\left(1 - M_m^2\right)\left(1 - M_n^2\right)}} & 1 \end{bmatrix}. \tag{2.35}$$

Solving equation (2.32) for function $A(T)$, we have

$$\Phi = \frac{A_0}{\sqrt{\det(\mathbf{Q})}}\sqrt{C_p}\exp\left(\int -\frac{\sigma}{2CC_p}\mathrm{d}T\right)\exp\left(\frac{\mathrm{i}\omega \mathbf{P}\mathbf{Q}^{-1}\mathbf{g}^{\mathrm{T}}}{2}\right)\exp(\mathrm{i}\omega T)\,. \tag{2.36}$$

The function σ in equation (2.36) is

$$\sigma = U_T\frac{\partial C_p}{\partial T} + U_T U_m\frac{\partial C_p}{\partial m} + U_T U_n\frac{\partial C_p}{\partial n}\,. \tag{2.37}$$

Equation (2.36) represents the final paraxial solution of the convected wave equation (2.17). In this solution, the function $\sqrt{\det(\mathbf{Q})}$ is analogous to the geometrical spreading in standard ray acoustics [11], which will determine the amplitude of the acoustic potential during the propagation process. The term $\exp\left(\int -\frac{\sigma}{2CC_p}\mathrm{d}T\right)$ reveals that the acoustic energy will also continually be transferred inside/outside the ray tubes during the propagation due to the flow inhomogeneity. However, in the atmosphere or underwater environments, the value of this term tends towards 1, and its influence is very small in the sound propagation process.

The matrix $\mathbf{P}\mathbf{Q}^{-1}$ manifests the variation of the wavefront curvature along the ray path, and the paraxial phase difference due to the wavefront curvature is included in the term $\exp\left(\frac{\mathrm{i}\omega \mathbf{P}\mathbf{Q}^{-1}\mathbf{g}^{\mathrm{T}}}{2}\right)$. Matrices $\mathbf{P}$ and $\mathbf{Q}$ are the solutions of the DRT equation (2.34), which can be efficiently solved by numerical methods for ordinary differential equations. The initial value of $\mathbf{P}$, $\mathbf{Q}$ at $T = T_0$ can be specified utilizing the similar procedure in quiescent media from Červený [12]. The solutions of the DRT equations will be real-valued, and we mark them as $\mathbf{P_A}$, $\mathbf{Q_A}$.

In the high-frequency asymptotic, discard all the ω^{-1}terms in equation (2.18), then the relationship between P and Φ is

$$P \approx \sqrt{\frac{\rho}{\rho_r}}\frac{c}{c_p}\Phi. \tag{2.38}$$

This result is similar to the high-frequency asymptotic relationship between P and Φ given by Pierce [10].

(c) Paraxial Gaussian beams

When solving the DRT equation (2.34), det(**Q**) is equal to 0 at the caustics, leading to singularities in the solution of the acoustic velocity potential equation (2.36). To address this issue, Červený [12] provides a beam construction method in quiescent media by setting the initial values of **P** and **Q** as complex values. The real parts of the matrix $\mathbf{PQ}^{-1}$ control the shape of the phase-front of the beam, and the imaginary parts control the width of the beam, at the initial position $T = T_0$. These initial values provide complex solutions of the DRT equations, where det(**Q**) is always non-zero and the matrix $\mathrm{Im}(\mathbf{PQ}^{-1})$ is positive definite and symmetrical everywhere along the ray. The singularity problem at the caustics is evaded. With the increasing square of distance from ray, the amplitudes of the beam decrease exponentially. For this reason, these solutions are called paraxial Gaussian beams, and the corresponding matrices are marked as $\mathbf{P_G}$ and $\mathbf{Q_G}$.

Following a similar approach, we can construct the complex solutions of the DRT equation (2.34) in inhomogeneous non-dissipative flows. Here we consider the case when we take the location of a point sound source as the initial emanating point of the beam.

For three-dimensional problems, the initial values of $\mathbf{P_G}$ and $\mathbf{Q_G}$ at the source location are set as

$$\mathbf{Q_G}(T_0) = \begin{bmatrix} 1 & 0 \\ 0 & 1 \end{bmatrix}, \quad \mathbf{P_G}(T_0) = \begin{bmatrix} \frac{\mathrm{i}}{2}\kappa_1^2 & 0 \\ 0 & \frac{\mathrm{i}}{2}\kappa_2^2 \end{bmatrix}, \tag{2.39}$$

where κ_1, κ_2 are arbitrary positive parameters. These initial values represent that the wavefront curvature radius at the source location is zero, and the widths of the three-dimensional Gaussian beam are specified by the positive parameters κ_1 and κ_2.

For two-dimensional problems, the matrices $\mathbf{P_G}$, $\mathbf{Q_G}$ regress into scalar functions P_G, Q_G. Referring to the construction method described by Červený [12] and [13], the 2 × 2 fundamental matrix **K** for the linearly independent real solutions of the DRT equation (2.34) is

$$\mathbf{K}(T) = \begin{bmatrix} Q_1(T) & Q_2(T) \\ P_1(T) & P_2(T) \end{bmatrix}, \tag{2.40}$$

where the two sets of solutions Q_1, P_1 and Q_2, P_2 can be specified by the following initial conditions:

$$\mathbf{K}(T_0) = \begin{bmatrix} 1 & 0 \\ 0 & 1 \end{bmatrix}. \tag{2.41}$$

Any complex solutions of the DRT equation (2.34) can be expressed in terms of the two linearly independent real solutions as follows

$$Q_G(T) = a_1 Q_1(T) + \mathrm{i}a_2 Q_2(T), \quad P_G(T) = a_1 P_1(T) + \mathrm{i}a_2 P_2(T), \tag{2.42}$$

where a_1 and a_2 are arbitrary positive parameters. Substitute equation (2.42) into the acoustic velocity potential solution equation (2.36), the two-dimensional Gaussian beam along the ray path is constructed and a_1/a_2 specifies the width of the beam at the initial position $T = T_0$.

(d) Gaussian beam summation in moving media

To compute the sound pressure at the observer, contributions of all vicinal beams should be summated. The three-dimensional Gaussian beam summation formula has the general form

$$P(\boldsymbol{x}) = \int\int W(\gamma_1, \gamma_2) P_{ray}(\boldsymbol{x_r}) \exp(\mathrm{i}\omega\tau(\boldsymbol{x}, \boldsymbol{x_r}))\, \mathrm{d}\gamma_1 \mathrm{d}\gamma_2, \tag{2.43}$$

where $P_{ray}(\boldsymbol{x_r})$ is the sound pressure at the point $\boldsymbol{x_r}$ on the ray path nearest to the observer position $\boldsymbol{x}$. Function $\tau(\boldsymbol{x}, \boldsymbol{x_r})$ expresses the wave propagation time from $\boldsymbol{x_r}$ to $\boldsymbol{x}$. The γ_1, γ_2 are the ray parameters specifying different rays in the integration. These parameters are defined as the azimuth and elevation angles of the group velocity vector $\boldsymbol{c_g}$ at the initial location of the ray path. It should be noted that, for the same observer location $\boldsymbol{x}$, the point $\boldsymbol{x_r}$ is different for different rays.

The function $W(\gamma_1, \gamma_2)$ is the weighting function used to describe different beams' contributions at the observer. Referring to the derivation of the weighting function in quiescent media by Červený [12], and considering the effect of the background flows, the revised weighting function is

$$W(\gamma_1, \gamma_2) = \frac{\omega}{2\pi}(-\det\mathcal{M})^{0.5} \frac{C_g}{C_p} |J|, \tag{2.44}$$

where the matrix $\mathcal{M} = \mathbf{P_G Q_G^{-1}} - \mathbf{P_A Q_A^{-1}}$, and $|J|$ represents the cross-sectional area of the ray tube normalized by $\mathrm{d}\gamma_1 \mathrm{d}\gamma_2$. The function $|J|$ can be calculated from the ray geometry, based on the equation (2.3). The functions C_g and C_p are the corresponding wave group speed and phase speed at the point $\boldsymbol{x_r}$ on the ray, and the coefficient C_g/C_p represents the revised factor for the convection effect.

Similar to the three-dimensional condition, the two-dimensional Gaussian beam summation formula is

$$P(\boldsymbol{x}) = \int W(\gamma_1) P_a(\boldsymbol{x_r}) \exp(\mathrm{i}\omega\tau(\boldsymbol{x}, \boldsymbol{x_r}))\, \mathrm{d}\gamma_1 . \tag{2.45}$$

The corresponding two-dimensional Gaussian beam summation weighting function is

$$W(\gamma_1) = \left(\frac{\omega}{2\pi}\right)^{0.5} (-\mathrm{i}\det\mathcal{M})^{0.5} \frac{C_g}{C_p} |J| . \tag{2.46}$$

Note that for the limiting case of infinitely wide Gaussian beams where $\mathrm{Im}(\mathbf{PQ^{-1}}) = \mathbf{0}$, the solution (2.36) will represent the standard paraxial ray approximation [12]. In quiescent media, the summation of paraxial ray approximations in three-dimensional models and in two-dimensional models yields results close or equal to the Maslov–Chapman theory [12,22]. And in one-dimensional models (vertically inhomogeneous, stratified quiescent media), the summation of paraxial ray approximations will yield the WKBJ (G. Wentzel, H. A. Kramers, L. Brillouin and H. Jeffreys) integral [23,24].

Therefore, by solving the RT equation (2.3) and the DRT equation (2.34), the paraxial acoustic potential can be obtained from equation (2.36). Based on the DRT equations, the paraxial Gaussian beams solution along the ray path can be constructed. Using the Gaussian beam summation equation (2.43) or (2.45), the sound pressure at the observer can finally be obtained. These are the major equations of the proposed GBT method in inhomogeneous flows. When there is no flow, these equations will reduce to the GBT equations derived by Červený [12] in quiescent media.

(e) Correction on sound attenuation due to the medium absorption

The sound attenuation due to the medium absorption is important for the high-frequency sound propagations over long distances [25]. This dissipation of the acoustic energy is due to viscosity, relaxation processes, thermal conduction and other processes [11]. It is not included in the GBT model in this work, since the governing equations are derived from the linearized Euler equations of fluid dynamics [10] and the acoustic medium is regarded as non-dissipative. However, for the long-distance sound propagations in the atmosphere or ocean, there are attenuation models that fit well into the ray tracing and beam tracing frameworks and can be efficiently implemented to our proposed GBT method.

Considering the sound attenuation during propagation outdoors for example, ISO 9613-1 [26] provides the method to calculate the sound absorption by the inhomogeneous atmosphere in a variety of meteorological conditions. In the frequency domain, the absorption loss $\delta L(f)$ along the sound propagation path is obtained by the following summation over the n segments

$$\delta L(f) = \sum_{i=1}^{n} \alpha_i(f)\, \delta s_i, \tag{2.47}$$

where $\alpha_i(f)$ is the average attenuation coefficient for atmospheric absorption at a frequency f, at the midpoint of the i^{th} path segment of length δs_i. From the ray tracing equation (2.3), the path segment length δs_i can be easily estimated.

The sound pressure P'_{ray} on the ray path is then corrected as

$$P'_{ray} = P_{ray}\, 10^{\frac{\delta L}{20}}, \tag{2.48}$$

where P_{ray} is the original value of sound pressure on the ray without consideration of the atmospheric absorption.

For the sound attenuation in seawater of the ocean, similar formulas can be established by applying the ocean attenuation models referring to [27,28] and [29].

(f) Time-domain broadband pulse propagation in moving media

In the preceding discussions, we focused on the monochromatic sound wave propagations in inhomogeneous flows. Similar to the procedures used in quiescent media [30] and [31], the time-domain GBT method for the acoustic broadband pulse propagation in inhomogeneous flows can be set up.

The sound pressure spectrum $P_0(\boldsymbol{x_0}, f)$ at the source $\boldsymbol{x_0}$ is first calculated by the Fourier transform of the given time-domain signal $p_0(\boldsymbol{x_0}, t)$. Then, the sound pressure spectrum $P_1(\boldsymbol{x_1}, f)$ at the observer $\boldsymbol{x_1}$ is computed by the GBT method for each frequency f. An inverse Fourier transform is performed to obtain the time-domain sound signal at the observer

$$p_1(\boldsymbol{x_1}, t) = 2\mathrm{Re}\int_0^{\infty} P_1(\boldsymbol{x_1}, f)\, e^{-\mathrm{i}2\pi f t}\, \mathrm{d}f\,. \tag{2.49}$$

Here we use the positive frequencies f in the Fourier integral to ensure the validity of the Gaussian beam solution equation (2.36) and the Gaussian beam summation formula equation (2.43).

In the calculation, only the Gaussian beam summation formula (2.43) is frequency-dependent, which implies the wave diffraction and scattering phenomena at different sound frequencies. The RT equation (2.3) and DRT equation (2.34) are frequency-independent and can be used for each frequency, which indicate the efficiency of the GBT method in computing the time-domain broadband pulse propagation.

It should be noted that the proposed GBT method is valid for pulse propagations in steady-state media. The impacts of unsteady flows on sound propagations cannot be captured, and

royalsocietypublishing.org/journal/rspa Proc. R. Soc. A 481: 20240485

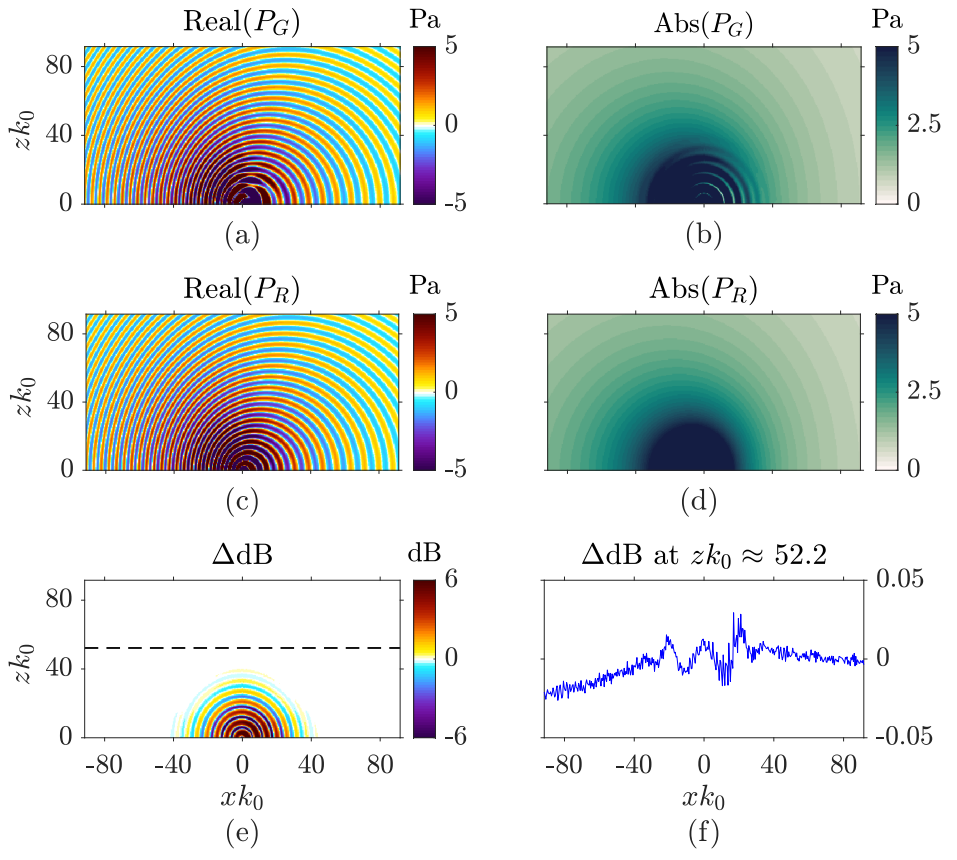

Figure 2. The sound pressure field of an acoustic monopole $f = 100$ Hz in a three-dimensional uniform flow $\boldsymbol{u_0} = (0.3\, c_0, 0, 0)$. (a) Real part and (b) amplitude of the sound pressure P_G calculated by the GBT method. (c) Real part and (d) amplitude of the sound pressure analytical solution P_R. (e) Error of the calculated sound pressure ΔdB. (*f*) ΔdB in the line $zk_0 \approx 52.2$, which is the dashed line in graph (e).

further investigations are required if this method is applied to evaluate the sound propagations in time-varying flows.

3. Validation case study

In this section, several benchmark problems of the sound wave propagations in moving non-dissipative media are investigated to validate the proposed GBT method. We define P_G as the sound pressure field computed by the GBT method, and P_R as the reference results obtained by the analytical solutions or the high-fidelity numerical results using the FEM or the FFP. The relative deviation ΔdB, and absolute deviation ΔPa between the GBT method and the reference results are defined as

$$\Delta\text{dB} = 20\log_{10}\frac{|P_G|}{|P_R|}, \quad \Delta\text{Pa} = |P_G| - |P_R|\,. \tag{3.1}$$

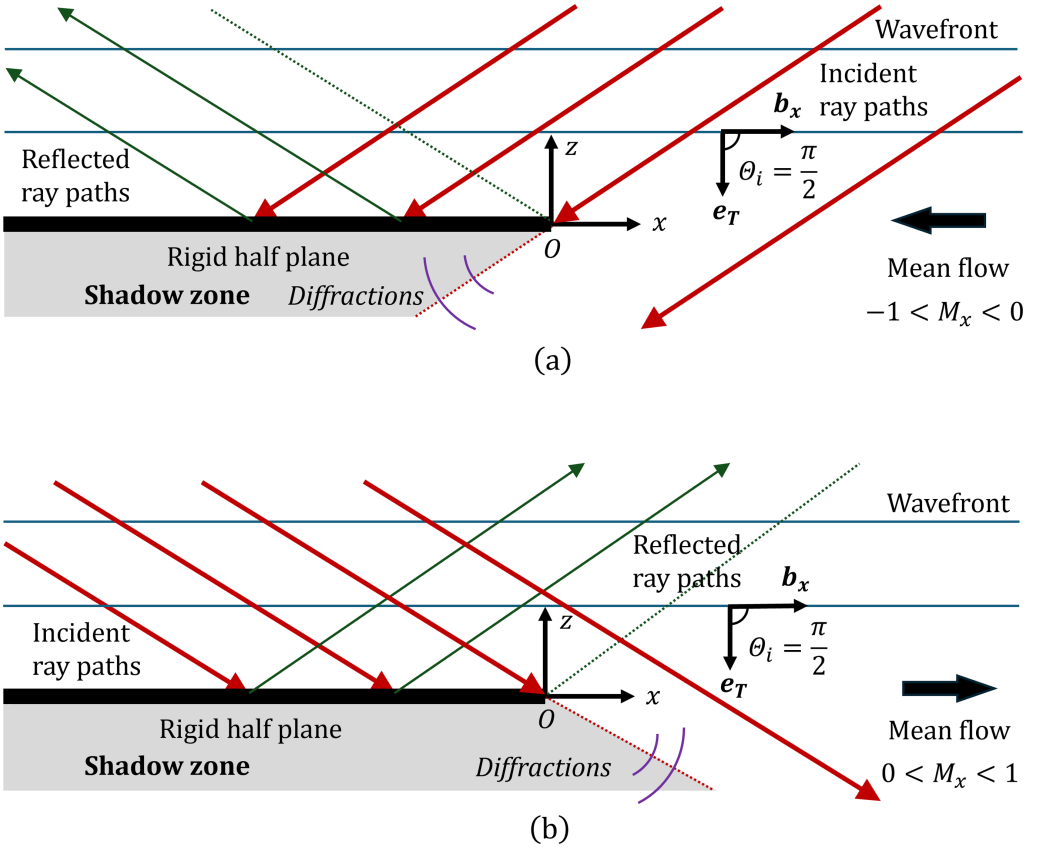

Figure 3. Sketch of the scattered plane wave by a rigid semi-infinite plane in a uniform mean flow. (a) The mean flow is in the $-\boldsymbol{b_x}$ direction. (b) The mean flow is in the $\boldsymbol{b_x}$ direction.

(a) The acoustic monopole in a three-dimensional free space uniform flow

In this benchmark problem, we consider the sound propagation in a three-dimensional free space uniform flow. A time harmonic acoustic monopole with the frequency $f = 100$ Hz is set at $\boldsymbol{x_s} = \boldsymbol{0}$. The medium sound speed $c_0 = 343\ \mathrm{m\,s^{-1}}$, and the density $\rho_0 = 1.21\ \mathrm{kg\,m^{-3}}$. In the Cartesian coordinates system (x, y, z), the uniform flow velocity is $\boldsymbol{u_0} = (0.3\,c_0,\ 0,\ 0)$. In this study, we define the reference wavenumber $k_0 = 2\pi f/c_0$, and the radial distance $r = |\boldsymbol{x} - \boldsymbol{x_s}|$, where $\boldsymbol{x}$ is the observer position.

The sound pressure results on the plane $y = 0$ are shown in figure 2. The analytical solution P_R is given by Ostashev [8], and the GBT method solution P_G is computed using the wide Gaussian beams with parameters $\kappa_1 = \kappa_2 = 0.0076$ in equation (2.39). In the far-field region $k_0 r > 50$, the error is less than 0.05 dB, demonstrating high computational accuracies of the proposed GBT method in this standard model.

In the near field $k_0 r < 30$, the large error of the GBT method is observed. Narrow beams are required for this near field region. These characteristics are the same as the GBT method results without flows [12]. In the following studies, we will follow the same beam parameters setting criteria used in the quiescent media.

(b) The two-dimensional semi-infinite rigid plane diffraction in a uniform flow

For the two-dimensional semi-infinite rigid plane diffraction and scattering of a plane wave in a uniform flow, there are known analytical solutions provided by Candel [32]. In a

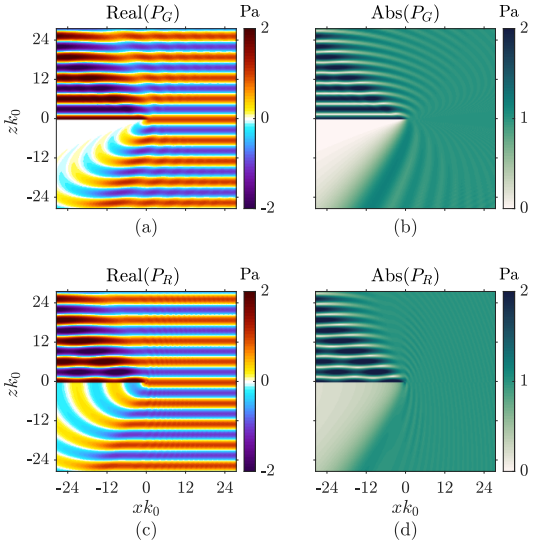

Figure 4. The rigid semi-infinite plane diffraction and scattering of a plane wave in a uniform flow $M_x = -0.8$. (a) Real part and (b) amplitude of the sound pressure P_G given by the GBT method. (c) Real part and (d) amplitude of the sound pressure analytical solution P_R.

two-dimensional Cartesian coordinates system (x, z), a semi-infinite rigid plane is located at $-\infty < x \leq 0$, $z = 0$. The velocity of a uniform flow is $\boldsymbol{u} = (u_x, 0)$, where c_0 is the medium constant sound speed. The corresponding Mach number is $M_x = u_x/c_0$.

A plane wave is incident on this semi-infinite plane with the incidence angle $\Theta_i \in (0, \pi)$ defined as the angle between the wavefront normal direction $\boldsymbol{e_T}$ and the Cartesian coordinates system basis vector $\boldsymbol{b_x}$. The schematic of the problem is shown in figure 3. In this case, we consider the plane wave incidence angle $\Theta_i = \pi/2$ with the angular frequency $\omega = 200\pi$ rad s^{-1}, pressure amplitude $|P| = 1$ Pa. The cases of $M_x = 0.8$ and $M_x = -0.8$ are studied. The analytical solutions P_R can be obtained from the work of Candel [32].

In the GBT method, referring to [12] and [33], the initial values of Q_A, P_A on each beam of the two-dimensional plane wave at an initial wavefront $T_0 = 0$ are specified as

$$Q_A(0) = 1, \quad P_A(0) = 0\,. \tag{3.2}$$

Solving the DRT equation (2.34) and applying the two-dimensional Gaussian beam construction formula (2.42), we obtain functions of P_A, Q_A and P_G, Q_G for each beam

$$Q_A(T) = 1, \quad P_A(T) = 0, \tag{3.3}$$

$$Q_G(T) = a_1 + \mathrm{i}a_2 c_0 c_p T, \quad P_G(T) = \mathrm{i}a_2, \tag{3.4}$$

where a_1, a_2 are the beam parameters, and $c_p = c_0 + u_x \cos\Theta_i$ represents the phase speed.

Following the equations (2.45) and (2.46), the two-dimensional plane wave Gaussian beam integration formula is obtained. In this diffraction problem, we construct the narrow Gaussian beams [12] with the beam parameters $a_1 = 1$ and $a_2 = 3.7 \times 10^{-4}$.

Comparisons of the GBT method solutions P_G and the analytical results P_R are shown in figures 4 and 5 when $M_x = -0.8$. In figure 5, it is demonstrated that the GBT method can successfully predict the wave diffraction, scattering and interference, as well as the directivities at different radial distances $k_0 r = 10$ and $k_0 r = 20$, where $r = |\boldsymbol{x}|$. Since the two quantities k_0 and r appear as a whole variable $(k_0 r)$ in analytical solutions [32], it reveals that the GBT method can also predict diffraction behaviours at different wave frequencies (the wavenumber k_0 will change correspondingly). It manifests the advantage of the GBT method over the standard

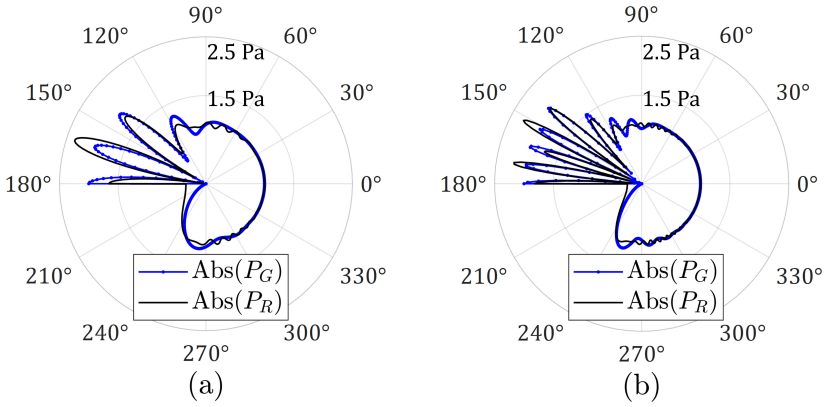

Figure 5. The sound pressure directivity comparisons between the GBT method result P_G and analytical solution P_R with $M_x = -0.8$, at the radius distances of (a) $k_0 r = 10$ and (b) $k_0 r = 20$.

ray acoustics, as it can successfully predict the sound pressure field diffraction at different frequencies.

The results comparisons for the flow $M_x = 0.8$ are shown in figures 6 and 7. Similar observations and conclusions can be obtained. It should be noted that, when the flow is in the $+\boldsymbol{b}_x$ direction, the analytical solutions [32] will include the pressure field of the shed vortex sheet at the semi-infinite plane trailing edge, and the sound pressure is singular at $\boldsymbol{x} = 0$. This result reveals the coupling between the acoustic and vorticity modes [34], and it cannot be captured by the GBT method, which is pure acoustics. However, the pressure field of the shed vortex sheet decays as $r^{-1/2}$ when $r \to \infty$, the deviation between the GBT method and analytical solution is small and can be ignored in the far-field regions.

(c) Sound propagation in a two-dimensional inhomogeneous stratified flow

The sound wave propagation in an inhomogeneous stratified flow is widely studied in underwater and atmospheric acoustics [4,6,8]. We will first consider the two-dimensional case in a Cartesian coordinates system (x, z), where the spatial distributions of the medium sound speed $c(z)$, flow velocity $\boldsymbol{u} = (u_x(z), 0)$ and density $\rho(z)$ are in the Sigmoid functions form

$$c(z) = \begin{cases} c_0\left(1 + A_C - \dfrac{A_C}{1+\exp\left(\frac{-z-L_0}{D_0}\right)}\right), & z \le 0 \\ c_0\left(1 + A_C - \dfrac{A_C}{1+\exp\left(\frac{z-L_0}{D_0}\right)}\right), & z > 0 \end{cases}, \tag{3.5}$$

$$u_x(z) = \begin{cases} c_0\left(M + A_M - \dfrac{A_M}{1+\exp\left(\frac{-z-L_0}{D_0}\right)}\right), & z \le 0 \\ c_0\left(M + A_M - \dfrac{A_M}{1+\exp\left(\frac{z-L_0}{D_0}\right)}\right), & z > 0 \end{cases}, \tag{3.6}$$

$$\rho(z) = \frac{\gamma p_0}{c^2(z)}. \tag{3.7}$$

The parameters L_0, D_0 represent the characteristic spatial lengths variations of the medium states, and the parameters A_C, M, A_M represent the corresponding characteristic magnitudes.

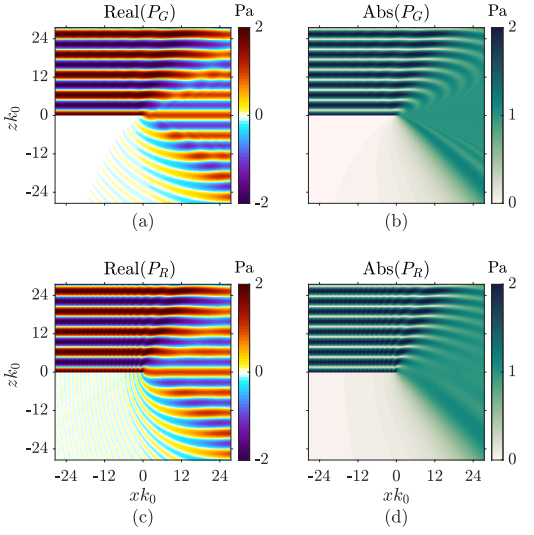

Figure 6. The rigid semi-infinite plane diffraction and scattering of a plane wave in a uniform flow $M_x = 0.8$. (a) Real part and (b) amplitude of the sound pressure P_G given by the GBT method. (c) Real part and (d) amplitude of the sound pressure analytical solution P_R.

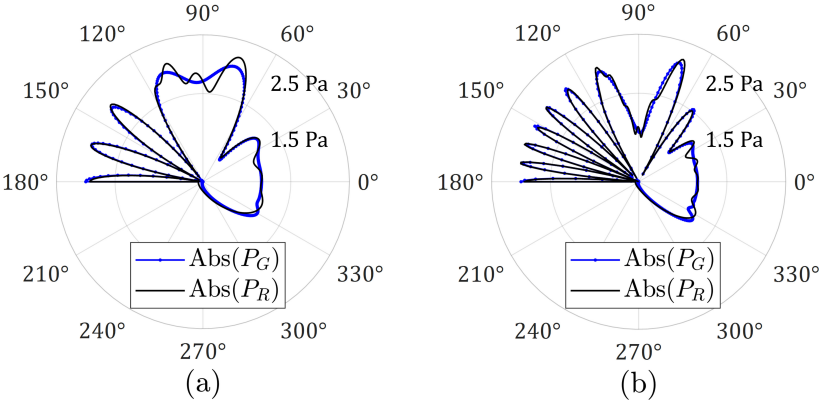

Figure 7. The sound pressure directivity comparisons between the GBT method result P_G and analytical solution P_R with $M_x = 0.8$, at the radius distances of (a) $k_0r = 10$ and (b) $k_0r = 20$.

The medium reference values are $c_0 = 343$ m s^{-1}, $p_0 = 101325$ Pa, $\gamma = 1.4$ and $\rho_0 = 1.21$ kg m^{-3}. In this work, the characteristic parameters are set as

$$L_0 = 45.80/k_0,\ D_0 = 3.66/k_0,\ A_c = 0.175,\ M = 0.0875,\ A_M = 0.175,$$

where $k_0 = 2\pi f/c_0$ is the reference wavenumber, and f is the sound wave frequency.

If a rotating acoustic dipole is set at $\boldsymbol{x_s} = \mathbf{0}$ with $f = 100$ Hz, then the sound pressure field can be completely determined. The dimensionless medium state functions $M_x = u_x/c$, c/c_0 and ρ/ρ_0 are plotted in figure 8a, and the corresponding ray paths are shown in figure 8b. The sound pressure field P_G computed by the GBT method, and the reference results P_R based on solving the linearized Euler equations via the FEM are shown in figure 9.

The result reveals that the proposed GBT method is competent to give an accurate solution both in regular regions and at caustics. It can also predict the wave interference patterns between the direct and refracted waves. In shadow zones (approximately in regions $xk_0 > 130$, and $40 < |zk_0| < 80$, as shown in the ray path in figure 8b), the result is not accurate, which is

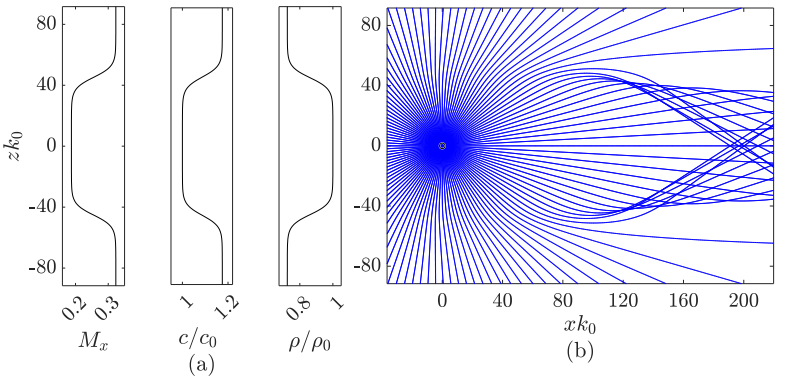

Figure 8. The sound propagation in a two-dimensional inhomogeneous stratified flow. (a) Medium state functions changing with zk_0. (b) Ray paths when the sound source locates at the origin.

caused by the choices of Gaussian beam parameters. According to Červený [12], wide Gaussian beams will yield the accurate sound field at caustics, but they are inaccurate for the diffractions in shadow zones. The diffraction calculation requires the use of very narrow beams. This inconsistency of the Gaussian beam parameter selection is the main disadvantage of the GBT method.

Figure 9e,f shows the deviations in the results obtained from the GBT method and the FEM. In most regions, the deviations are within 3 dB. In shadow zones and destructive interference regions, the deviations can be high up to 5 dB. The reason is that the sound pressures are inherently low in these areas. If we investigate the absolute deviation ΔPa in the results obtained by the GBT method and the FEM, it is actually small, as shown in figure 9f.

(d) Sound propagation in a three-dimensional inhomogeneous stratified flow

In this subsection, we will study the sound wave propagation in a three-dimensional inhomogeneous stratified flow with the rigid boundary condition. We apply the same setting of the atmosphere surface layer airflow used by Wilson [6]. In the three-dimensional Cartesian coordinates system (x, y, z), the spatial distribution of the wind profile $\boldsymbol{u} = (u_x(z), 0, 0)$ is in the logarithmic function form

$$u_x(z) = \begin{cases} 0, & z \le 0.05 \text{ m} \\ \dfrac{u_*}{k_a} \ln \dfrac{z}{z_0}, & z > 0.05 \text{ m} \end{cases} \tag{3.8}$$

where u_* is the friction velocity, $k_a \approx 0.4$ is the von Kármán's constant and z_0 is the roughness length. The value used for $u_* = 0.6\ \text{m s}^{-1}$, is typical of the atmospheric surface layer in neutrally buoyant, windy conditions. The value used for $z_0 = 0.05$m, is typical of long grass ground [35]. The air sound speed and density are constant with $c_0 = 343\ \text{m s}^{-1}$, and $\rho_0 = 1.21\ \text{kg m}^{-3}$.

An acoustic monopole source is placed at $\boldsymbol{x_s} = (0, 0, 6)$ m, with the frequency $f = 400$ Hz, and the normalized strength is $Q = 4\pi/(-2i\pi f\rho_0)$. The observer $\boldsymbol{x}$ is set at the plane $z = 1.8$ m. The ground at the plane $z = 0$ is modelled as a planar rigid boundary in this validation study. The schematic sketch of this sound propagation scenario is shown in figure 10. Applying the reflection model used in the classical ray tracing method [8] and [12], the reflected beams can be calculated. The overall sound field is the superposition of the direct and reflected Gaussian beams contributions.

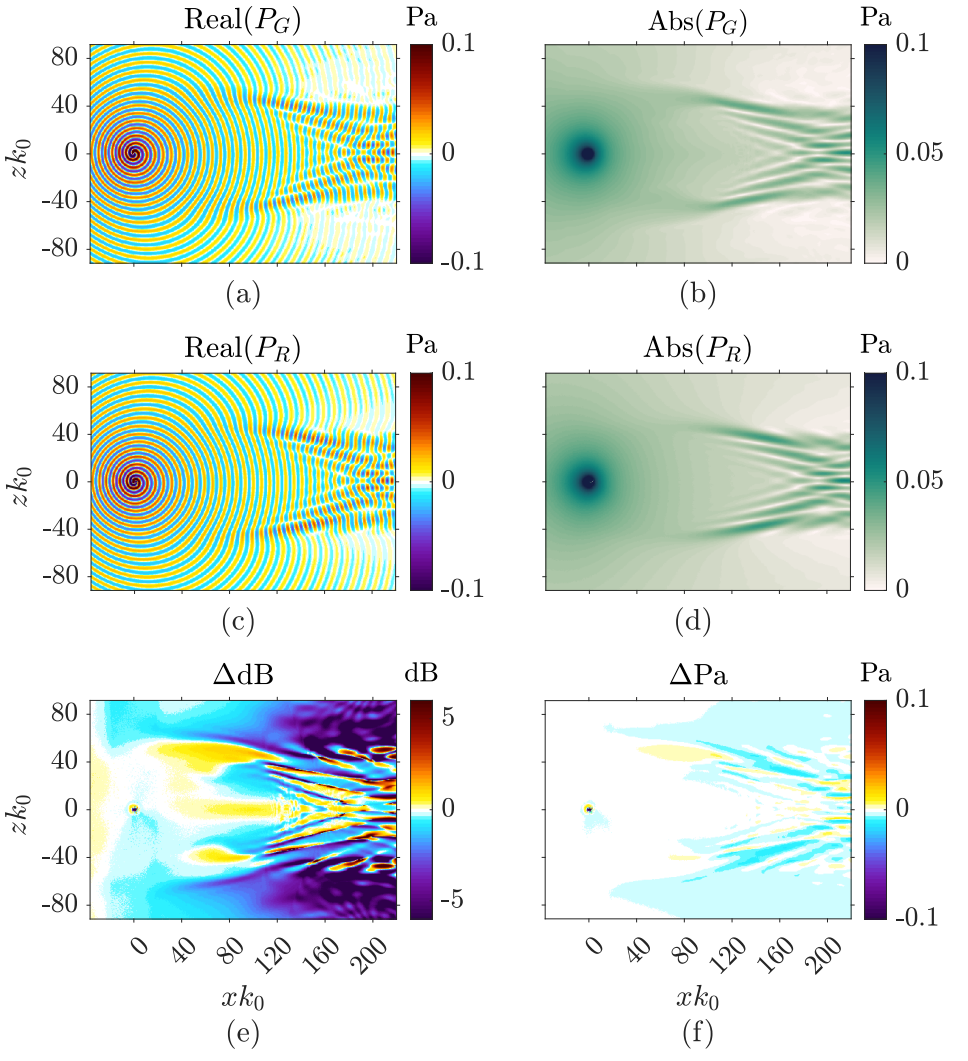

Figure 9. The sound propagation in a two-dimensional inhomogeneous stratified flow. (a) Real part and (b) amplitude of the sound pressure P_G obtained by the GBT method. (c) Real part and (d) amplitude of the sound pressure P_R obtained by the FEM. (e) Relative deviation ΔdB and (f) absolute deviation ΔPa of the sound pressure amplitude.

The wind profile $u_x(z)$ is plotted in figure 11a, and the corresponding ray paths are shown in figure 11b,c. The sound pressure field P_G computed by the GBT method, and the reference result P_R based on the high-fidelity numerical FFP, are shown in figures 12 and 13.

These results demonstrate that the GBT method can accurately predict the interference patterns formed by the direct and reflected acoustic waves in the three-dimensional non-uniform flow, and precisely compute the wave refractions phenomena due to the flow inhomogeneity. For example, in the ray paths diagram (figure 11b), in the region $x \in (-60, -40)$ m and $z \in (0, 2)$ m, there are wave caustics formed by the ray upward refractions in the wind profile. The corresponding sound pressure augmentations in this region can be successfully captured by the GBT method, as shown in figures 12a and 13a.

The result is less accurate in the near source region ($|\boldsymbol{x} - \boldsymbol{x}_s| \le 5$ m), since the wide Gaussian beam parameters $\kappa_1 = \kappa_2 = 0.0076$ in equation (2.39) are applied for the far-field radiation

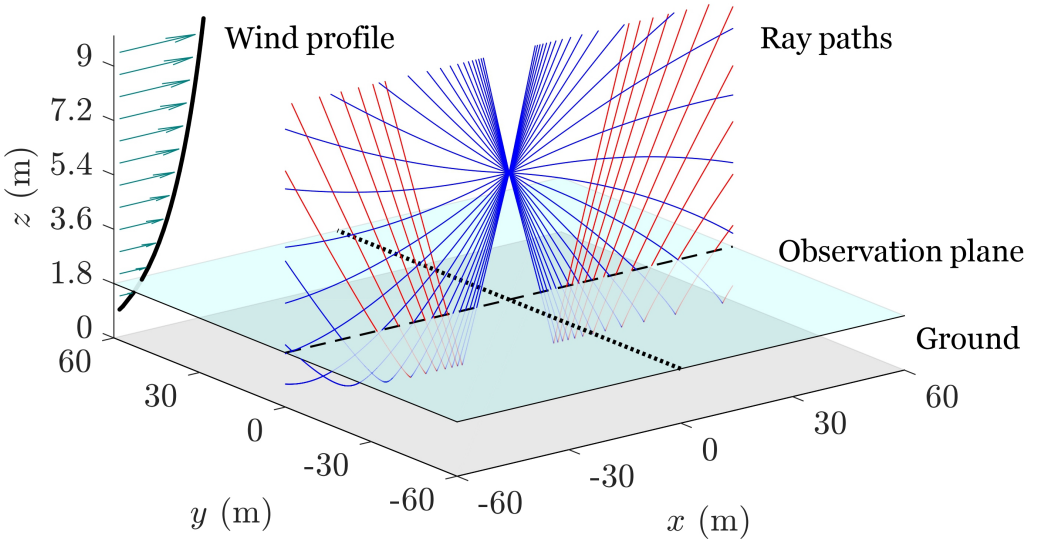

Figure 10. The sound propagation scenario in a three-dimensional stratified flow. The blue paths are the direct acoustic rays, and the red paths are the reflected acoustic rays.

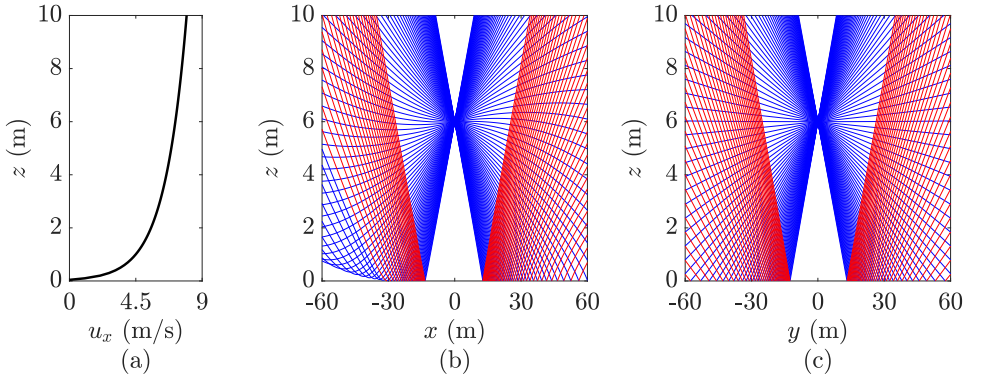

Figure 11. The sound propagation in a three-dimensional inhomogeneous stratified flow with the planar rigid boundary. (a) The wind profile function changing with the height z. (b) Ray paths in the xz plane at $y = 0$, and (c) ray paths in the yz plane at $x = 0$. The blue paths are the direct rays, and the red paths are the reflected rays.

calculations. This beam parameters selection criterion is the same as the calculations used in the quiescent media [12], as discussed in §3a.

The impact of the non-uniform flow on the sound wave propagation is also revealed in figure 12. The amplitude of the sound pressure $P_{uniflow}$ in a uniform wind is shown in figure 12c, which is calculated by the analytical method [8]. The constant flow value is set as the wind speed at the source location $u_x = (u_*/k_a)\ln((6\text{ m})/z_0) \approx 7.18\text{ m s}^{-1}$, with the Mach number $M_{x0} \approx 0.02$. Compared with figure 12a,b, it can be clearly seen that the far-field sound radiations have large derivations between the non-uniform flow and uniform flow conditions. The impact of the flow inhomogeneity on the sound propagation cannot be ignored even if the flow Mach number is much less than 1.

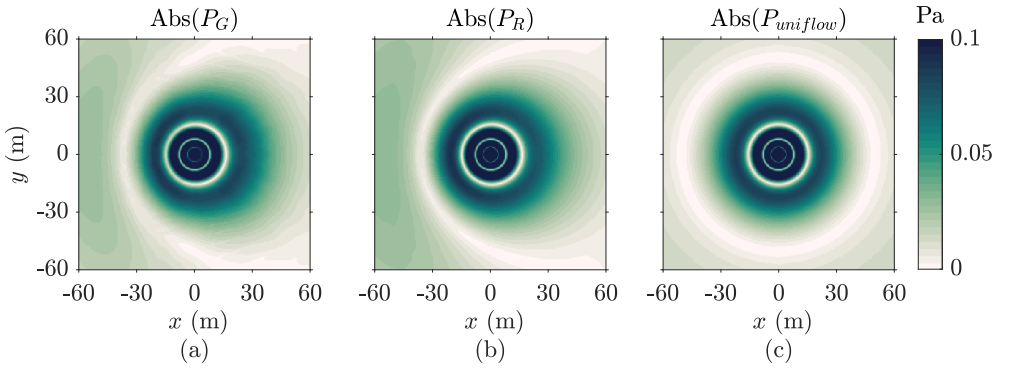

Figure 12. The sound pressure field at the xy plane with the height of $z = 1.8$ m. (a) The amplitude of the sound pressure P_G obtained by the GBT method. (b) The amplitude of the sound pressure P_R obtained by the FFP method. (c) The amplitude of the sound pressure $P_{uniflow}$, obtained by the analytical solution, when the wind profile is ignored.

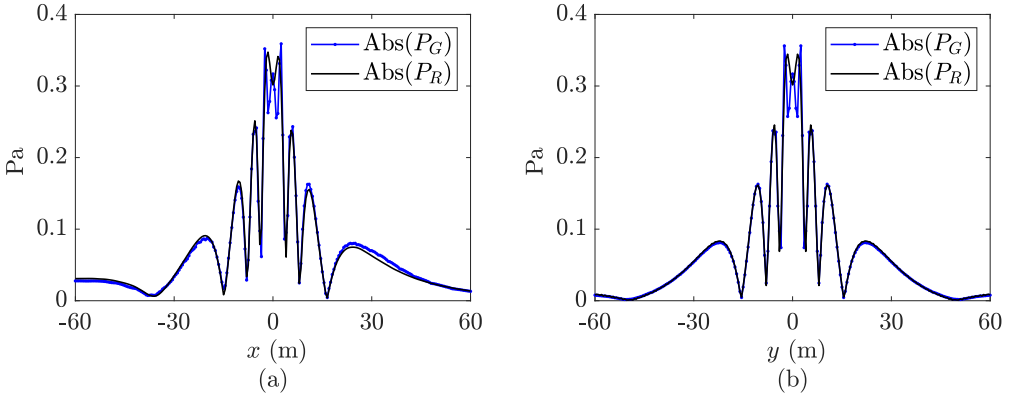

Figure 13. The sound pressure distributions on the xy plane at the height of $z = 1.8$ m. (a) In the parallel wind direction, in the line $y = 0$ (which is the dashed line in figure 10). (b) In the crosswind direction, in the line $x = 0$ (which is the dotted line in figure 10).

(e) Sound propagation in a two-dimensional inhomogeneous stratified flow

The large-scale vortex flow is one of the typical air flow patterns in the urban atmosphere environment [36]. In this case, we consider the sound wave propagation in a simplified two-dimensional vortex flow field. In a Cartesian coordinates system (x, z), we define the flow velocity field $\boldsymbol{u}(u_x, u_z)$ as

$$u_x = -A_M c_0 (z - z_0) \exp\left(-\frac{\left(\sqrt{x^2 + (z - z_0)^2} - R \right)^2}{\sigma^2} \right), \tag{3.9}$$

$$u_z = A_M c_0 x \exp\left(-\frac{\left(\sqrt{x^2 + (z - z_0)^2} - R \right)^2}{\sigma^2} \right), \tag{3.10}$$

where the parameters z_0, R, σ represent the characteristic spatial lengths variations of the vortex flow, and the parameter A_M represents the corresponding characteristic magnitude. The

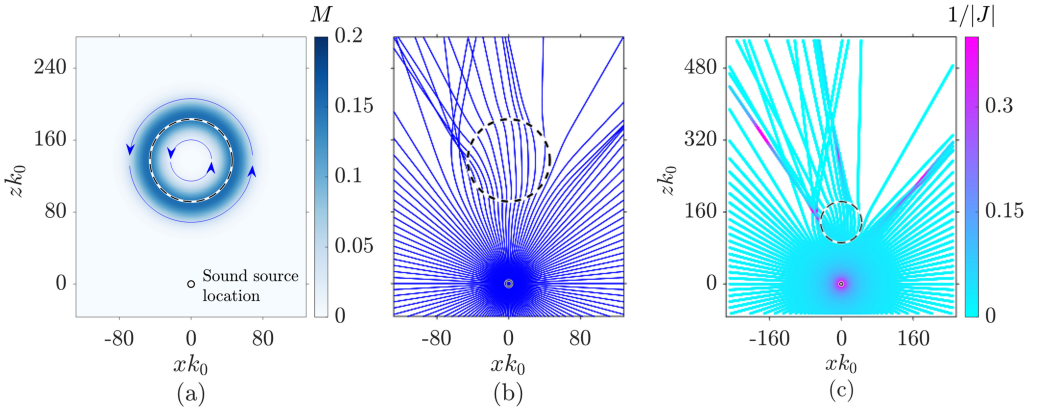

Figure 14. The two-dimensional sound propagation in a vortex flow. (a) Background flow velocity distribution. The dashed line indicates the locations of the highest flow magnitude. (b) Ray paths when the sound source locates at origin. (c) Ray paths in a larger domain, and the values $1/|J|$ along the ray paths. The function $|J|$ is the normalized cross-sectional area of the ray tube. The points in magenta colour indicate the locations of the caustics.

medium sound speed $c_0 = 343$ m s^{-1} and density $\rho_0 = 1.21$ kg m^{-3} are constant. In this work, the characteristic parameters are set as

$$z_0 = 137.39/k_0,\ R = 45.80/k_0,\ \sigma = 18.32/k_0,\ A_M = 0.058,$$

where $k_0 = 2\pi f/c_0$ is the reference wavenumber, and f is the sound wave frequency.

If an acoustic dipole in the $\boldsymbol{e_z}$ direction is set at $\boldsymbol{x_s} = \boldsymbol{0}$ with $f = 200$ Hz, then the sound pressure field can be completely determined. The flow magnitude $M = |\boldsymbol{u}|/c_0$ spatial distribution is shown in figure 14a and the corresponding ray paths are plotted in figure 14b. The sound pressure field P_G computed by the GBT method, and the reference results P_R based on solving the linearized Euler equations via the FEM, are shown in figure 15.

The result reveals that the proposed GBT method is competent to give an accurate solution in both regular regions and at caustics. It can also predict the wave interference patterns between different refracted rays in the non-parallel background flow (vortex flow in this case). This provides an advantage over the FFP method, which is only applicable to scenarios of layered acoustic media [8]. If the accuracy in shadow zones is ignored, the sound pressure amplitude relative deviation ΔdB is generally less than 3 dB. Large relative deviations occur in destructive interference regions, where the reference sound pressure amplitudes are inherently small. The absolute deviation ΔPa in the results obtained by the GBT method and the FEM is still not large, as shown in figure 15f.

Figure 16 shows the sound pressure distributions on the straight line $zk_0 \approx 155.71$ passing through caustics, and on the straight line $zk_0 \approx 274.77$ behind the vortex flow area. Strong sound wave refractions caused by the vortex flow can be observed, despite the relatively low flow velocity in this study (the maximum flow Mach number $M_{\max} \approx 0.15$). In addition, there are caustics formed even in the no-flow regions away from the vortex flow area, which demonstrate the 'flow lens effect' on sound wave propagations, as shown in figure 14c. Therefore, the impacts of the non-uniform flows on the acoustic field are complex and generally cannot be ignored in underwater or atmospheric acoustics studies.

(f) Broadband pulse propagation in a two-dimensional free space uniform flow

In the preceding validations, we studied the monochromatic sound wave propagations in inhomogeneous flows. This subsection will discuss the acoustic broadband pulse propagation

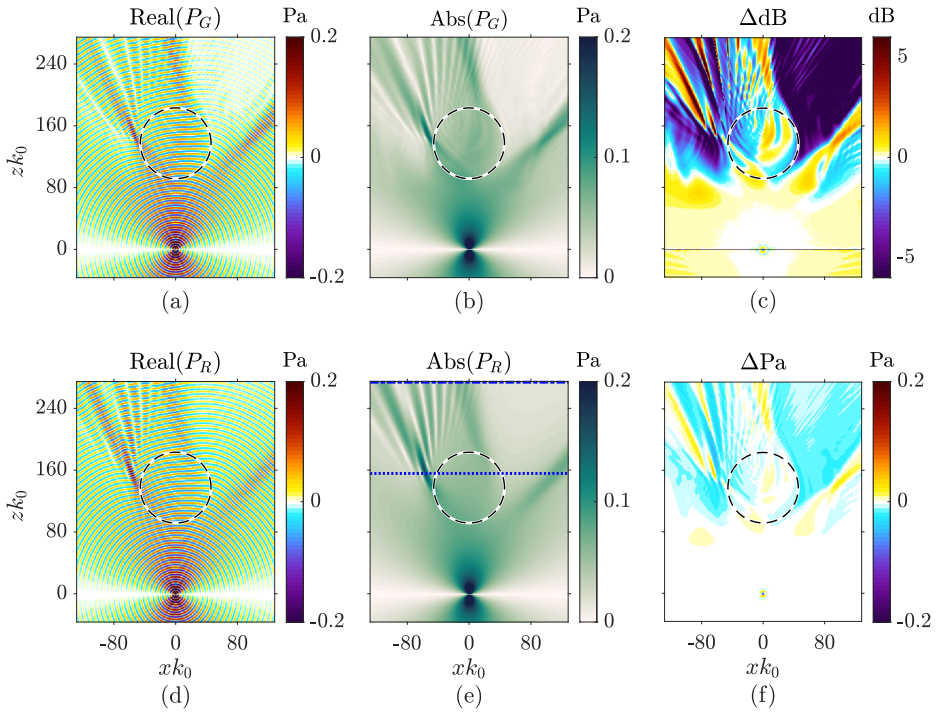

Figure 15. The sound propagation in a two-dimensional vortex flow. (a) Real part and (b) amplitude of the sound pressure P_G obtained by the GBT method. (d) Real part and (e) amplitude of the sound pressure P_R obtained by the FEM. (c) Relative deviation ΔdB and (f) absolute deviation ΔPa of the sound pressure amplitude.

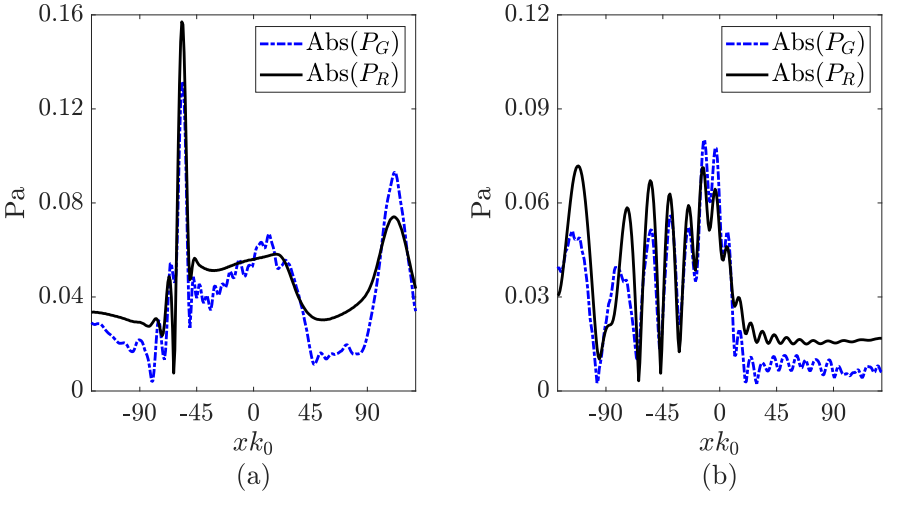

Figure 16. The sound pressure distributions, (a) in the line $zk_0 \approx 155.71$ (which is the dotted line in figure 15*e*) passing through a caustic, and (b) in the line $zk_0 \approx 274.77$ (which is the dashed line in figure 15e) behind the vortex flow area.

in a two-dimensional free space uniform flow, as a benchmark for the time-domain GBT method.

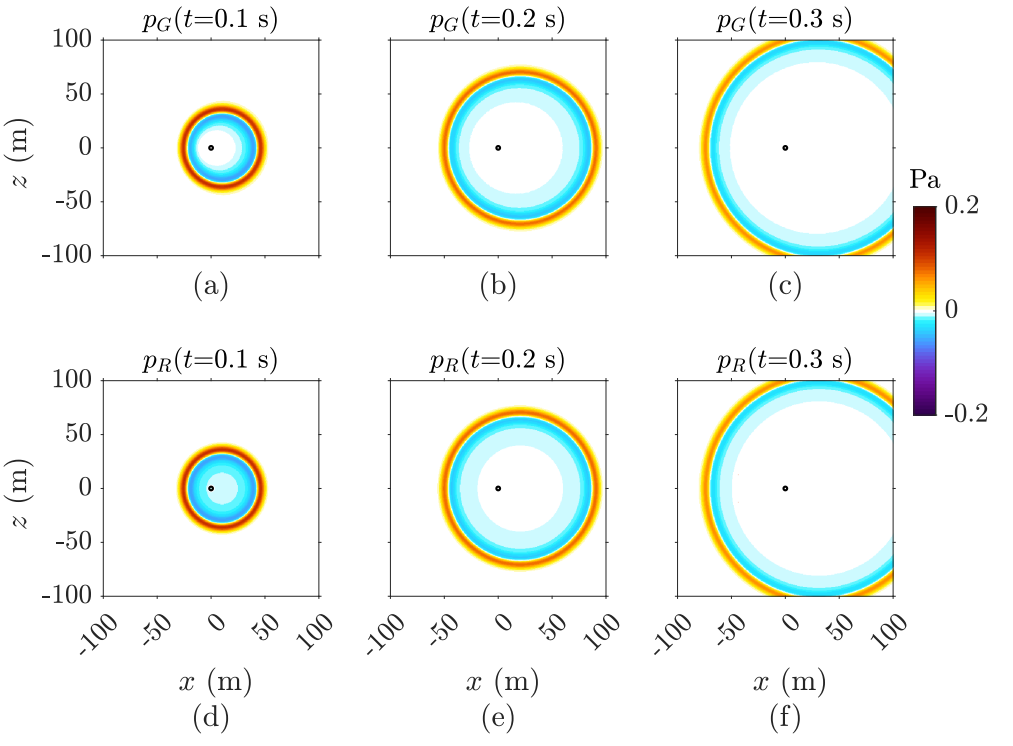

Figure 17. The sound pulse propagation in a two-dimensional uniform flow. Graphs (a,b) and (c) are the sound pressure p_G given by the GBT method, at the times $t = 0.1$ s, $t = 0.2$ s and $t = 0.3$ s. Graphs (d,e) and (f) are the corresponding analytical solutions p_R.

In a two-dimensional Cartesian coordinates system (x, z), we consider an acoustic pulse generated by an initial Gaussian distribution of the sound pressure at the time $t = 0$ with the initial value

$$p_0 = e^{-\alpha(x^2+z^2)} \text{ Pa}, \tag{3.11}$$

where $\alpha = \ln(2)/\beta^2$, $\beta = 3.43$ m. The initial value of the acoustic perturbation velocity is $\boldsymbol{v} = \boldsymbol{0}$. The pulse propagates in a uniform flow $\boldsymbol{u} = (M_x c_0, 0)$, where $M_x = 0.3$, and the medium sound speed $c_0 = 343$ m s^{-1}. The analytical solution of this problem p_R is given by [37].

In the GBT method, based on the symmetric initial conditions, the propagation of the diverging broadband pulse during the time $t > 0$ can be described by beams emanating from a virtual point source at the origin. The time-domain GBT method described in §2f is performed to compute the sound signal at an observer $\boldsymbol{x_{ob}}$. For the far-field sound radiation, the wide Gaussian beam parameters $a_1 = 100$, $a_2 = 0.0029$ are applied following the criteria given in [30].

The results p_G calculated by the time-domain GBT method and their comparisons with the analytical solution p_R are depicted in figures 17 and 18. Due to the selection of the wide beam parameters, the computed sound pressure is less accurate in the near source origin ($|\boldsymbol{x_{ob}}| < 10$ m). However, for the observer at a larger distance, the proposed GBT method is capable of providing reliable predictions for the sound pressure responses.

Figure 19 shows the sound pressure spectrum P_G calculated by the GBT method and the analytical solution P_R, at the location (50 m, 0) and (100 m, 0), respectively. For this uniform flow, the characteristic length of ambient quantities variations is infinitely large, far exceeding

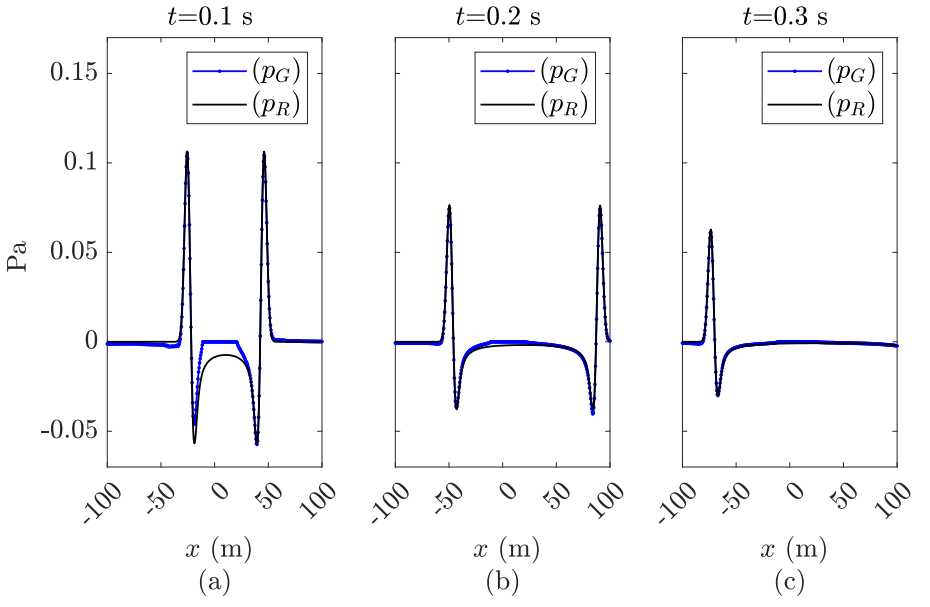

Figure 18. The sound pressure waveform along the x-axis in a two-dimensional uniform flow. Graphs (a), (b) and (c) show the sound pressure in the line $z = 0$ at the times $t = 0.1$ s, $t = 0.2$ s and $t = 0.3$ s.

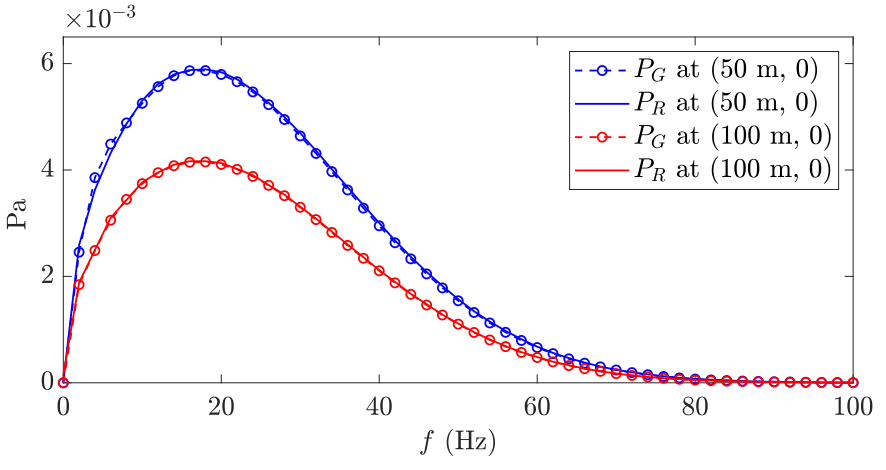

Figure 19. The sound pressure spectrum in a two-dimensional uniform flow, at (50 m, 0) and (100m, 0).

the characteristic wavelengths of sound waves. Therefore, the high-frequency approximation is valid for sound waves at all frequencies. Consequently, the GBT method can accurately capture the sound pressure at each frequency contained in the broadband pulse. Additionally, in this non-dissipative medium, the attenuation of sound during the propagation is solely due to the geometrical spreading [12], which is consistent for all frequencies. Therefore, there is no acoustic dispersion, and the waveform remains unchanged during the propagation.

4. Conclusion

This paper presents an improved Gaussian beam tracing method to model the sound wave propagation in inhomogeneous flows. In the ray acoustics framework, the dynamic ray tracing equations are derived from the convected acoustic velocity potential wave equation under the high-frequency asymptotic and paraxial approximations in the wavefront orthogonal coordinate system along the ray path. The solutions of the acoustic potential and corresponding Gaussian beams are developed. The sound pressure at the observer is accurately computed by superimposing all vicinal beams, through a revised weighting function that considers the convection effect on each beam. For validation, this method is applied to several benchmark problems and the results are compared with the analytical solutions (when applicable) and the high-fidelity numerical results. At most observer locations, good agreements are obtained with the reference solutions. In certain regions, the deviation of the sound pressure level can be high. However, it is caused by the inherently low sound pressures in these regions, such as in the shadow zones or destructive interference regions. In these case studies, it has been shown that the impact of the flow inhomogeneity on the sound propagation cannot be ignored even if the flow Mach number is much less than 1, and the proposed Gaussian beam tracing method is competent in tackling the long-distance sound propagations in the presence of non-uniform flows where neither the analytical solutions nor the conventional high-fidelity numerical results are feasible.

Data accessibility. This article has no additional data.

Declaration of AI use. We have not used AI-assisted technologies in creating this article.

Authors' contributions. H.B.: conceptualization, formal analysis, methodology, validation, visualization, writing - original draft; Q.T.: investigation, software, validation, visualization; P.Z.: conceptualization, investigation, supervision, writing - review and editing; W.C.: investigation, supervision, validation; X.Z.: conceptualization, investigation, methodology, resources, supervision, writing - review and editing; S.Z.: conceptualization, formal analysis, investigation, supervision, writing - review and editing.

All authors gave final approval for publication and agreed to be held accountable for the work performed therein.

Conflict of interest declaration. We declare we have no competing interests.

Funding. H.B. is supported by a studentship from the Hong Kong University of Science and Technology. Part of this work is supported by the Hong Kong Research Grant Council (RGC. 16206422 and 25201624).

References

1. Nomura T, Takagi K, Sato S. 2010 Finite element simulation of sound propagation concerning meteorological conditions. *Int. J. Numer. Methods Fluids* **64**, 1296–1318. (doi:10.1002/fld.2444)
2. Ostashev VE, Wilson DK, Liu L, Aldridge DF, Symons NP, Marlin D. 2005 Equations for finite-difference, time-domain simulation of sound propagation in moving inhomogeneous *media* and numerical implementation. *J. Acoust. Soc. Am.* **117**, 503–517. (doi:10.1121/1.1841531)
3. Dinapoli F, Deavenport R. 1979 Ocean Acoustics. In Topics in current physics series. Springer-Verlag.
4. Jensen FB, Kuperman WA, Porter MB, Schmidt H, Tolstoy A. 2011 Computational ocean acoustics. vol. **2011**. Springer.
5. Raspet R, Lee SW, Kuester E, Chang DC, Richards WF, Gilbert R, Bong N. 1985 A fast-field program for sound propagation in a layered atmosphere above an impedance ground. *J. Acoust. Soc. Am.* **77**, 345–352. (doi:10.1121/1.391906)
6. Wilson DK. 1993 Sound field computations in a stratified, moving medium. *J. Acoust. Soc. Am.* **94**, 400–407. (doi:10.1121/1.407051)

7. Salomons EM. 2001 *Computational atmospheric acoustics*. Springer Science & Business Media.
8. Ostashev VE, Wilson KD. 2015 *Acoustics in moving inhomogeneous media*. CRC Press. (doi:10.1201/b18922)
9. Landau LD, Lifshitz ME. 2013 *Fluid mechanics: Landau and Lifshitz: course of theoretical physics*. vol. **6**. Elsevier.
10. Pierce AD. 1990 Wave equation for sound in fluids with unsteady inhomogeneous flow. *J. Acoust. Soc. Am.* **87**, 2292–2299. (doi:10.1121/1.399073)
11. Pierce AD. 2019 Acoustics: an introduction to its physical principles and applications. Springer.
12. Červený V. 2001 *Seismic ray theory*. vol. **110**. Cambridge, UK: Cambridge University Press.
13. Červený V, Popov MM, Pšenčík I. 1982 Computation of wave fields in inhomogeneous *media* -- Gaussian beam approach. *Geophys. J. Int.* **70**, 109–128. (doi:10.1111/j.1365-246x.1982.tb06394.x)
14. Porter MB. 2019 Beam tracing for two- and three-dimensional problems in ocean acoustics. *J. Acoust. Soc. Am.* **146**, 2016–2029. (doi:10.1121/1.5125262)
15. Bian H, Fattah R, Zhong S, Zhang X. 2020 An efficient rectilinear Gaussian beam tracing method for sound propagation modelling in a non-turbulent *medium*. *J. Acoust. Soc. Am.* **148**, 4037–4048. (doi:10.1121/10.0002966)
16. Bian H, Fattah R, Zhong S, Zhang X. 2021 On the efficient modeling of generic source directivity in Gaussian beam tracing. *J. Acoust. Soc. Am.* **149**, 2743–2751. (doi:10.1121/10.0004318)
17. Yunus F, Casalino D, Avallone F, Ragni D. 2023 Efficient prediction of airborne noise propagation in a non-turbulent urban environment using Gaussian beam tracing method. *J. Acoust. Soc. Am.* **153**, 2362. (doi:10.1121/10.0017825)
18. Červený V, Pšenčík I. 2010 Gaussian beams in inhomogeneous anisotropic layered structures. *Geophys. J. Int.* **180**, 798–812. (doi:10.1111/j.1365-246X.2009.04442.x)
19. Chen YC, Zhang HG, Zhang MH, Yang SE. 2023 Gaussian beam tracing for three-dimensional sound propagation problems in subsonic moving *medium*. *Acta Phys. Sin.* **72**, 124301. (doi:10.7498/aps.72.20221691)
20. Ostashev VE, Wilson DK, Muhlestein MB. 2020 Wave and extra-wide-angle parabolic equations for sound propagation in a moving atmosphere. *J. Acoust. Soc. Am.* **147**, 3969. (doi:10.1121/10.0001397)
21. Červený V, Pšenčík I. 1983 Gaussian beams and paraxial ray approximation in three-dimensional elastic inhomogeneous media. *J. Geophys.* **53**, 1–15.
22. Klimeš L. 2002 The relation between Gaussian beams and Maslov asymptotic theory. *Stud. Geophys. Et Geod.* **46**, 85–95. (doi:10.1023/a:1024806029177)
23. Chapman CH. 1976 Exact and Approximate Generalized Ray Theory in Vertically Inhomogeneous *Media*. *Geophys. J. Int.* **46**, 201–233. (doi:10.1111/j.1365-246x.1976.tb04154.x)
24. Chapman CH. 1978 A new method for computing synthetic seismograms. *Geophys. J. Int.* **54**, 481–518. (doi:10.1111/j.1365-246x.1978.tb05491.x)
25. Blackstock D. 2000 Fundamentals of physical acoustics. Wiley-Interscience.
26. ISO 9613-1. 1993 Acoustics-Attenuation of sound during propagation outdoors-Part 1: Calculation of the absorption of sound by the atmosphere. Standard International Organization for Standardization
27. Francois RE, Garrison GR. 1982 Sound absorption based on ocean measurements. Part II: Boric acid contribution and equation for total absorption. *J. Acoust. Soc. Am.* **72**, 1879–1890. (doi:10.1121/1.388673)
28. Ainslie MA, McColm JG. 1998 A simplified formula for viscous and chemical absorption in sea water. *J. Acoust. Soc. Am.* **103**, 1671–1672. (doi:10.1121/1.421258)
29. Fisher FH, Simmons VP. 1977 Sound absorption in sea water. *J. Acoust. Soc. Am.* **62**, 558–564. (doi:10.1121/1.381574)
30. Popov M. 2002 *Ray theory and Gaussian beam method for geophysicists*. Salvador-Bahia: EDUFBA.
31. Babich VM, Popov MM. 1989 Gaussian summation method (review). *Radiophys. Quantum Electron.* **32**, 1063–1081. (doi:10.1007/bf01038632)

32. Candel SM. 1973 Diffraction of a plane wave by a half plane in a subsonic and supersonic *medium*. *J. Acoust. Soc. Am.* **54**, 1008–1016. (doi:10.1121/1.1914311)
33. Červený V. 1982 Expansion of a plane wave into Gaussian beams. *Stud. Geophys. Et Geod.* **26**, 120–131. (doi:10.1023/A:1024849811430)
34. Rienstra SW. 1981 Sound diffraction at a trailing edge. *J. Fluid Mech.* **108**, 443–460. (doi:10.1017/s0022112081002206)
35. Panofsky HA, A.Dutton J. 1984 *Atmospheric turbulence. models and methods for engineering applications.* New York, NY: Wiley.
36. Hunter LJ, Watson ID, Johnson GT. 1990 Modelling air flow regimes in urban canyons. *Energy Build.* **15**, 315–324. (doi:10.1016/0378-7788(90)90004-3)
37. Tam CKW, Webb JC. 1993 Dispersion-relation-preserving finite difference schemes for computational acoustics. *J. Comput. Phys.* **107**, 262–281. (doi:10.1006/jcph.1993.1142)